Magnetic Field Focusing Design Guidelines for Long Range Position and Orientation Detection

Marcelo Ribeiro, Michael Ortner
Microsystem Technologies
CTR – Carinthian Tech Research
Villach, Austria
marcelo.ribeiro@ctr.at, michael.ortner@ctr.at

***Abstract* — In the context of magnetic position or proximity detection, to overcome the fast decay of the magnetic fields of permanent magnets, the application and construction of a field focusing device is studied. The "field focuser", as it is referred to, allow designers to increase distances between magnet and sensor, choose weaker and cheaper magnets and work with cost-efficient 1D magnetic sensors. Design and prototyping of such a sample focuser was covered in detail in previous publications [1, 2], which are partially reviewed here, with additional information on how to develop such a device based on experimental and FEM simulation studies. Critical parameters like materials, geometries, distances, movement ranges, magnets, sensors and readout systems and their influences and correlations are discussed in detail to improve the understanding of such systems and to support designers with the development of similar devices.**

Keywords- magnetic sensing; magnetic simulations; far magnetic field detection; field focusing; linear position detection

I. INTRODUCTION AND MOTIVATION

While magnetic field sensors and sensing principles have been around for a long time [3], the last decades have witnessed an explosion in the development of magnetic sensing technologies driven by the technological advance and a rapidly growing demand in industrial applications [4]. This development has been made possible by the numerous advantages provided by magnetic sensors over other measurement systems, such as small packaging sizes and miniaturization [5], low production costs, contactless measurement possibilities, high resolution [6], low power requirements and an excellent robustness against vibrations, temperature, moisture and dirt. Today's magnetic sensors have established themselves in every major industrial sector with applications ranging from mechanical orientation, position and motion sensing, magnetic material and state analysis and detection, via navigation and guidance systems to a variety of applications in medicine, archeology, space exploration and countless others [7, 8].

One of the great advantages when dealing with magnetic systems for orientation and position detection is that the magnet, being the field source, is in principle a passive component that requires no power supply and can thus easily be mounted on moving or enclosed parts.

When dealing with long distance position or proximity measurements using typical magnet-magnetic sensor systems based on Hall technology, one of the biggest difficulties is to achieve the magnetic field amplitudes, of the order of few tens of millitesla, required by the sensor manufacturers, e.g. [9]. This is due to the fact that the amplitude of the magnetic field *B(r)* of a permanent magnet generally decays like (1) for distances that are of the order of the size of the magnet or larger [10].

$$B(r) \sim \frac{M}{r^3} \tag{1}$$

Here *r* denotes the distance from the magnet and *M* denotes the magnetic moment which depends on the remanence field and the magnet geometry. As the field amplitude scales linearly with the magnetization, in general one cannot compensate the fast decay with the distance by choosing stronger magnets, as shown in Fig. 1.

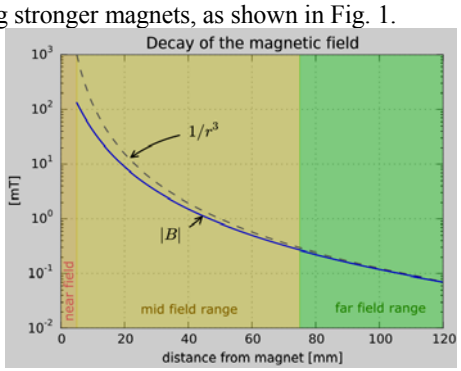

Figure 1. Decay of the magnetic field of a cylindrical permanent magnet.

The fast decay of the magnetic field along the axis of a cylindrical permanent magnet with a remanence field of B_r=1300mT is depicted in Fig. 1. Notice that in the immediate vicinity of the magnet the field is of the order of a few hundred millitesla, while in a distance of only 10cm it already drops to ~0.1mT.

For industrial applications, this fact is quite troubling as the prices of permanent magnets, especially the ones based on rare earth materials, make this system uneconomical when the distances that should be measured exceed few

centimeters. With the strong limitation given by the sensor's sensitivity, position and distance measurements are only feasible in the near field range.

If the limit is set by stray field amplitude rather than sensor sensitivity, the application ranges can be greatly improved. A typical stray field like the earth magnetic field is well below 100 microtesla which, if used as the limit in the above example, would improve the possible range from 20mm to 100mm.

In the this work, the development of a field focusing device to enhance weak magnetic fields for use with cost-effective Hall sensor technology is presented. This device allows designers to increase distances between magnet and sensor, choose weaker and cheaper magnets and work with simpler 1D magnetic sensors instead of more expensive 2D or 3D ones.

II. PROPOSED SOLUTION

To overcome the limitations when dealing with position and distance measurements, a field focusing device that allows one to detect the weak fields of permanent magnets at large distances is proposed. The focuser consists of a core made of a soft magnetic material of high permeability, which is divided into two pieces by a small gap with a magnetic field sensor placed inside. The underlying principle is that the highly permeable core attracts and enhances the weak external magnetic field, as outlined in the sketch in Fig. 2.

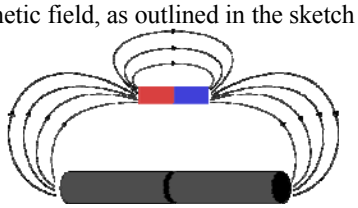

Figure 2. Sketch of the field focusing principle

If the gap is small, compared to the thickness of the core, the field propagation in the focuser can be described using magnetic circuit theory [11]. The two major effects are that the magnetic field in the core becomes homogeneous as the gap acts like a resistance, and that it propagates at full amplitude, enhanced by the core permeability, through the gap.

Such a setup, thus, enhances the magnetic field that can be picked up by the sensor, while being robust against positioning tolerances of the sensor inside the core's air gap.

The general idea of field focusing has already been studied in other contexts [12, 13]. In this work we focus on extreme far field detection and cost-effective implementation using 1D Hall sensor technology.

III. DESIGN PARAMETERS AND HINTS

A first step when designing a field focuser for a magnetic system is to define the measurement setup, then the type of sensor and readout system, and finally estimating the focuser parameters which fit the defined requirements.

A. *Desired measurement setup*

Magnetic position detection is realized by moving magnet and magnetic sensor relative to each other which results in a variation of the intensity of the sensor output signal for different positions or orientations, as depicted in the sketch in Fig. 3.

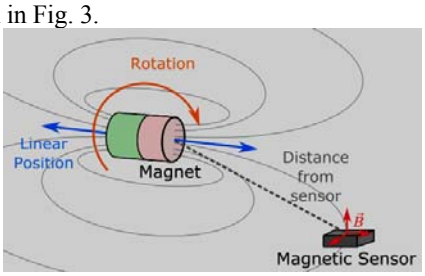

Figure 3. Sketch of a magnetic position and orientation detection setup

The association of a specific position or orientation to each of the values measured by the magnetic sensor is named the magnetic map, and depends on each setup, type of movement and position. The most common parameters of such setups are:

- Magnet:
  - Geometric shape
  - Dimension
  - Magnetization
  - Orientation
- Setup:
  - Airgap
  - Movement type and range
  - Required signal processing
  - Sensor
  - Desired resolution

B. *Sensor parameters and readout system*

There are several types of magnetic sensors available on the market. For 1D magnetic Hall sensors, there are some key parameters to be observed when choosing the appropriate model:

- Sensitivity:
  - Readout range (e.g. 10-200mT)
- Output type:
  - Analog (e.g. 0-5V)
  - Digital (e.g. SPI, I²C, CAN, etc.)
- Power supply:
  - Chip supply (usually 3-5V)
  - Power consumption (usually in the µA to mA range)

The readout system has to be defined either as a part of the overall system or must be based on the parameters of the sensor:

- Analog sensor output:
  - µC with ADC, USB ADC for PC, etc.
- Digital sensor output:

- μC, DSP, FPGA, etc.

C. Focuser design

The design of the focuser depends strongly on the characteristics of the magnet as well as the distances and the movement ranges involved. A weaker magnet and larger distances and movement ranges require a stronger focusing device.

- Airgap, movement range and type:
  - These are usually system requirements and the rest can be parameterized to work within what is defined here.
  - The distance between the sensor and the magnet, often referred to as the airgap, strongly influences the field amplitudes at the sensor, see (1).
- Magnet and sensor:
  - These are the components of the system which should be chosen and configured to fulfill the above requirements.
  - Smaller and weaker magnets are typically more cost-effective.
  - The sensors can be chosen for different ranges, but typical Hall type sensors work in the 10-200mT range.
  - Knowing the airgap, movement range, magnet and available sensor, one can calculate the resulting magnetic field along the sensing line and identify the lack of signal for the chosen sensor.
- Field focuser:
  - The focuser has several construction parameters such as dimensions, shape and material.
  - When choosing a shape, the manufacturing effort should be kept in mind.
  - The dimensions are related to the size of the sensor, the system airgap and the movement ranges of the measurement.
  - The most effective way to fabricate a focusing device is to place the sensor in-between two highly permeable cores. A constant slit much thinner than the core width for placing the sensor guarantees a homogeneous field of high intensity.
  - The dimensions of the cores should be approximately the size of the movement range in order to decrease distortions in the signal (e.g. if the magnet moves ±20mm the focuser should be at least 40mm long).
  - The cores should be made of a soft ferromagnetic material to avoid hysteresis effects and residual magnetization. The permeability is responsible for the field focusing or enhancement effect.

IV. CASE STUDY

While the initial idea of how to improve the magnetic field detection at greater distances is quite simple, the development of the focusing device was a step by step process that shall partly be reproduced here to improve understanding, for justification and argument of the final setup.

A. Auxiliary tools

In order to test and understand the system, magnetostatic simulations were performed using the FEM environment ANSYS Maxwell 16 [14], while experiments were executed with a self-developed system composed of a robot manipulator, a magnetic sensor, hardware, firmware and software that access sensor data and provide output files for further analysis.

1) FEM Simulation Environment

All simulations were performed using the FEM environment ANSYS Maxwell 16, designed to deal with low frequency electrodynamics. The environment attempts a solution via the magnetic field B. The underlying solution space is given by continuous piecewise second order polynomials on a mesh of tetrahedral element geometry. To obtain the respective basis functions, the fields are calculated for ten points, the node values at vertices and on the edges. The FEM matrix equation is solved using standard sparse matrix solution techniques like e.g. SGE or ICCG [15]. The local error is obtained from the non-zero part of the divergence of the magnetic field.

A special feature of ANSYS Maxwell is the adaptive mesh algorithm, which features a step by step refinement of the original mesh depending on the local error until a global error criterion defined by the user is reached. For all simulations, validity was ensured by observation of the global error of subsequent passes of 30% mesh refinement.

2) Experimental setup

The system consists of a robot arm with its controller (EPSON E2C351S), sensor readout units, magnetic sensors, integration software (CTR RAMSRS V1.0) and tools that can provide physical support for magnets and sensors. A detailed description of the experimental environment can be found in [16].

3) Sensor used

The sensor used was an MLX90215, configured to its highest sensitivity of 140mV/mT, and powered with 5V. The detection of positively oriented fields is expressed from 2.47V upwards, while the detection of negatively oriented fields from 2.47V downwards. The conversion of the sensor readout from Volts to Tesla is explained by (2). Further information can be found in [17].

$$B[\mathrm{mT}] = \frac{x[\mathrm{V}] - 2.47}{140 \cdot 10^{-3}} \tag{2}$$

Here x denotes the sensor output in Volt and B the magnetic flux density expressed in mT.

B. Initial simulations

The initial setup was based on an educated guess with the concept of Fig. 2 in mind. Previous observations suggest that the gap, that should be of the order of 1mm to hold a magnetic sensor, must be much smaller than the thickness of the core. The initial dimensions, presented in Fig. 4, were chosen in accordance with the dimensions of the available material for experimentation.

In the simulation the core was modeled with linearized material parameters, St37 Steel ($\mu_r = 2700$) and Iron ($\mu_r = 3000$), while the magnet was modeled as NdFeB ($B_r = 1.05T$ and $\mu_r = 1.007$) and SmCo ($B_r = 1.25T$ and $\mu_r = 1.17$).

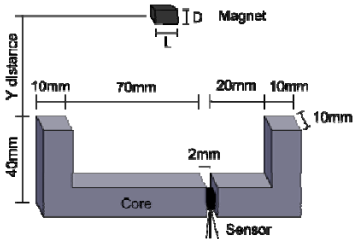

Figure 4. Initial dimensions of the model matching the experimental setup

The asymmetric positioning of the sensor air gap is due to the material available for the production of the first core prototype for the actual measurements, and the "U" shape was considered for better fitting of the core onto the actual "bent" form of the magnetic field lines, see Fig. 5.

Fig. 5 shows a snapshot of the magnetic field in such a setup from the FEM simulation using the previously introduced steel core and an NdFeB magnet.

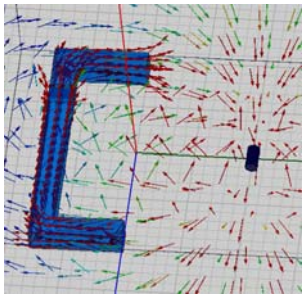

Figure 5. Initial simulation snapshot

As expected, the magnetic field lines were strongly focused inside the core even at large distances from the magnet. Results from the simulations using an iron core can be found in Table I.

C. Initial measurements

To confirm that the simulations were in accordance with the output given by real measurement devices, an experiment was conducted. In this experiment the magnets were placed manually using a simple non-magnetic magnet holder, and the core was constructed from laminated, soft magnetic transformer sheets. The magnetic field in the gap was read out with a magnetometer, Wuntronic Koshava [18].

While the experiment was of a crude nature, it draws advantage from the fact that sensor placement in the gap is quite stable against displacements. Results from the experiment are given in Table I.

D. Simulation and measurement result comparison

To reasonably compare simulation results and measurement outputs, the simulation material parameters were determined from one experiment with an airgap of 50mm. This was necessary to account for the unknown exact remanence fields of the magnets used in the experiment, and their possible demagnetization. All other distances were simulated using the same remanence field. The results for experiment and simulation are given in Table I.

TABLE I. SIMULATION VS. MEASUREMENT RESULTS

	Results			
	NdFeB - 18x12mm		***SmCo - 10x5mm***	
Dist.	**Sim. [mT]**	**Meas. [mT]**	**Sim. [mT]**	**Meas. [mT]**
5cm	5.99 ±0.5%	6.02 ±0.3mT	0.651 ±0.5%	0.64 ±0.03mT
7cm	3.20 ±0.5%	3.25 ±0.2mT	0.357 ±0.5%	0.36 ±0.03mT
9cm	1.82 ±0.5%	1.88 ±0.1mT	0.202 ±0.5%	0.21 ±0.03mT
11cm	1.12 ±0.5%	1.17 ±0.1mT	0.125 ±0.5%	0.14 ±0.03mT

Table I shows that experiment and simulation results are in good agreement and match with a maximal difference of only 10%, despite the simple experimental setup.

E. Core optimizations

After the concept was considered valid, an optimization phase was started aiming to find better dimension and material configurations. This optimization process was carried out in the simulation environment, which was considered reliable after the previous successful comparisons with the experiments.

The procedure consisted of trying different materials and dimensions for the core. The variables taken into account for optimization were the length of the core L, the thickness of the core D and the arm length of the core H, depicted in Fig. 6.

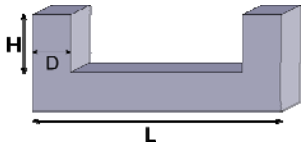

Figure 6. Variables varied during the core's optimization phase

The results from the simulations are presented in Fig. 7.

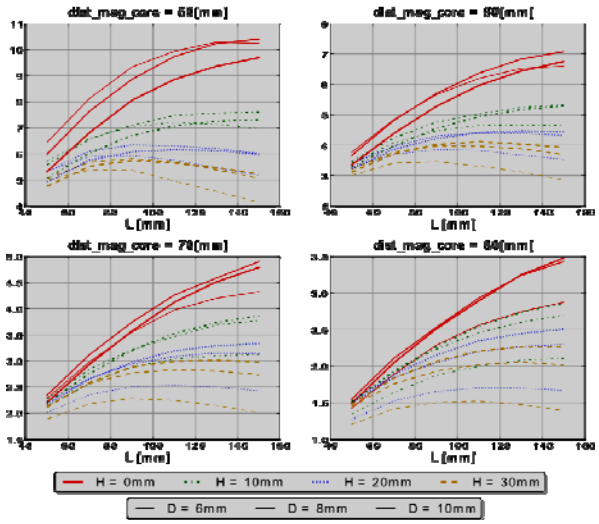

Figure 7. Core optimization charts

The traces show the strength of the magnetic field at the position of the sensor in units of millitesla. The four images show the results for four different distances between the magnet and the core. On the horizontal axis the length of the core L is varied from 50mm to 150mm. Different colors/line styles and different line thicknesses denote different arm lengths H and core thicknesses D respectively. One can immediately see the tendency that the field will be strongest when the arm length disappears. This can be understood as the absolute distance between the sensor and the magnet increases with the arm length. Other results, not so readily interpreted, are that the long cores seem to improve the field up to a certain point, and that thinner cores seem to work just as fine, sometimes even better, than thick ones.

While the optimal arm length H of the core is zero the optimal length L seems to depend on the core's thickness as well as the distance from the magnet. It is not very surprising that the optimal value is found for $H = 0$, as the above implementation fixes the distance between focuser and magnet, not between sensor and magnet. When it comes to core thickness it appears that thinner cores would increase the flux when there is no gap, however, for a fixed gap size of 1mm, the optimal thickness lies between 6 to 10mm.

Further simulations, where the shape of the core was analyzed, showed that a cylindrically shaped core, which is easier to manufacture and handle, shows a very similar behavior compared to the rectangular one.

A screenshot from the simulation environment with the cylindrical shape can be seen in Fig. 8.

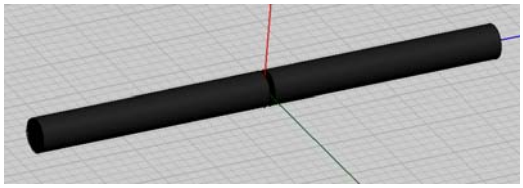

Figure 8. Final core shape

For the core material, simulations with variation of the material permeability (μ) were conducted. As expected from magnetic circuit theory, the magnetic field inside the gap should increase with the magnetic permeability of the core. The results are presented in Fig. 9.

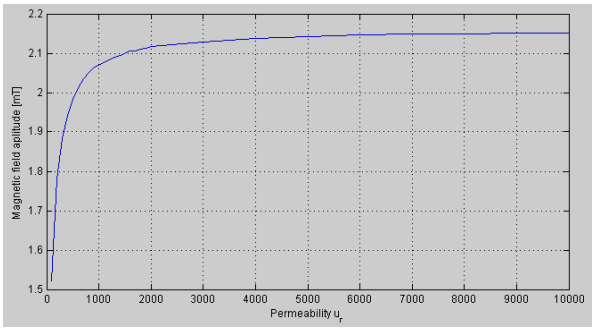

Figure 9. Core's relative permeability analysis

One can observe that the field increases until a permeability of approximately $\mu_r = 1000$ is reached, but little is gained by choosing values of μ_r beyond that. This is not a saturation effect but rather a result of the atan-behavior of the field enhancement with the permeability. From a cost point of view this can be interesting, as cheap steel or iron cores will bring almost similar gains as expensive high-end materials like mu-metal.

F. Focuser manufacturing

The core dimensions as well as the material characteristics based on the simulation outcomes were used to manufacture an according prototype, which can be seen in Fig. 10.

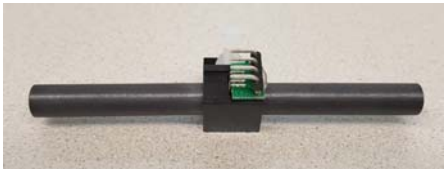

Figure 10. Final core prototype

The final design consists of two cylindrical pieces of ferrite with a relative permeability of $\mu_r \sim 2000$, a length of 43mm and a diameter of 6mm. It includes a plastic sensor holder, which holds the sensor and joins both core halves. Additionally, there is a hole where a screw can be placed to fixate the field focuser as an integrant of another system. All parts, except the core, are made of non-magnetic materials.

G. Analysis of the focuser

There were two approaches used to identify the field focuser's performance: one was measuring the increase of field in the slit where the sensor is placed, and the other was to check the deformation in the field in the vicinity of the focuser. While the first is a direct way of testing the performance, the second analysis brings a deeper

understanding of how the device distorts the magnetic field in its surroundings.

The measurements were analyzed by comparing data of the magnetic field amplitudes in presence and absence of the ferrite cores, both in terms of simulations and experiments.

A snapshot of the magnetic fields plotted in the simulation software, which illustrate the operation of the system, can be found in Fig. 11.

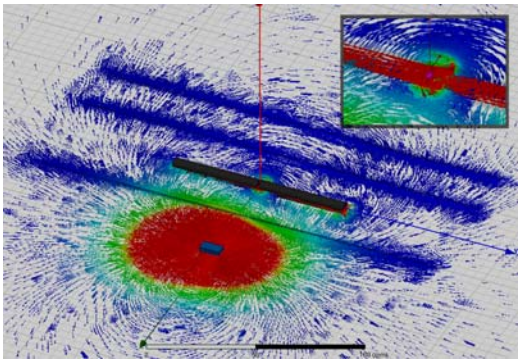

Figure 11. Magnetic field vectors in presence of the field focuser obtained by FEM simulation

The red areas represent strong magnetic fields and the blue areas weak magnetic fields. It is possible to see that the areas with high field amplitudes are concentrated around the magnet (as it is the source of the field) and inside the ferrite cores of the field focuser. In the vicinity of the sensing lines and the sensing point a higher concentration of vectors appears due to the finer mesh in these areas to achieve a higher resolution.

H. Signal increase in the focuser's core

Initial measurements were performed by placing a rectangular shaped magnet parallel to the field focuser and by moving it in X direction, as shown by the sketch in Fig. 12.

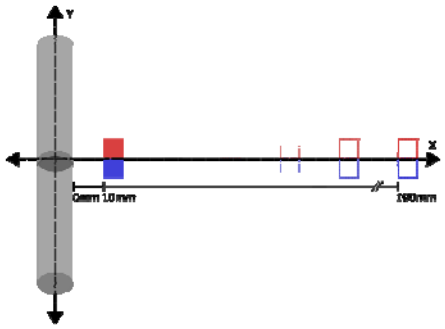

Figure 12. Sketch of the measurements for detecting the performance increase over distance

The measurements were carried out for airgaps of 10mm to 190mm, limited by the robot arm's operation range, with 10mm step size. The datasets for 19 positions, with proper averages of 100 respective measurements, for each of the four scenarios, simulation and experiment with and without the ferrite cores, are shown in Fig. 13.

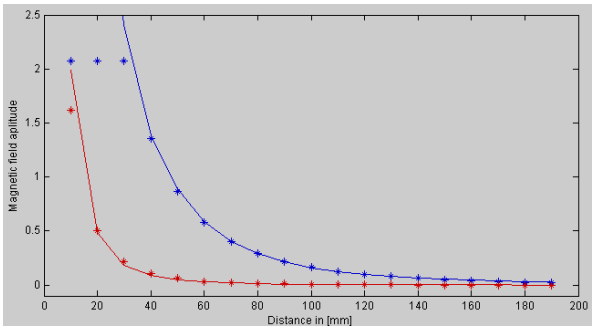

Figure 13. Results of the performance increase over distance in presence and absence of the field focuser

The solid lines represent the simulation results and the markers the experimental measurements. The red and blue traces correspond to setups with and without the ferrite cores respectively. Analyzing the chart, it is clear that the field focuser improves the measuring range, as the amplitude is enhanced on the whole range in the presence of the cores when compared to their absence, reassuring the validity of the proposed solution. The plateau of the sensor signal at small distances (blue markers) is a result of the saturation of the sensor, as for small airgaps the field exceeds the range of the latter. For practical application this is unproblematic as the system is intended for long range measurements.

The field focusers performance is obtained by comparing the measurements in presence and absence of the focuser and is shown in Fig. 14.

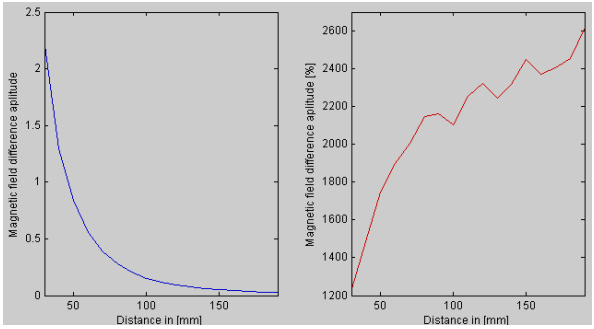

Figure 14. Difference between the signal with and without the ferrite cores extracted from simulations

The blue trace represents the absolute difference between the signal with and without the ferrite core, and the red trace the relative improvement of the signal strength in the presence of the cores.

The above results are promising, but for real world applications signal-to-noise ratios of the readout system are critical when dealing with weak signal amplitudes. The sensors used in the experiments have noise levels ranging from $8mV_{pp}$ to $60mV_{pp}$ ($50mV_{pp}$ for the used configuration), limiting the measurement range to signals above the noise threshold. Fig. 15 shows a semi-logarithm plot of the simulated results with a reference line representing the sensor noise threshold.

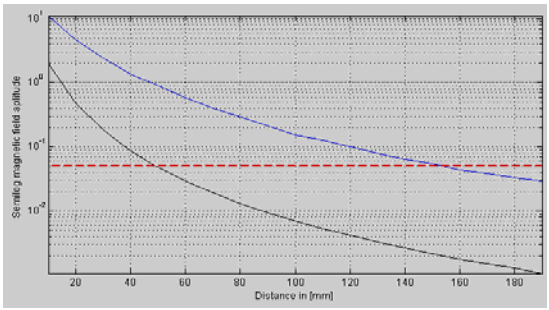

Figure 15. Performance comparison over distance with noise threshold

The blue and black traces show the signal in presence and absence of the ferrite cores respectively. The red dashed line represents the sensor's noise barrier. Measurements with this setup without the focuser are limited to distances of ~45mm, while in the presence of the cores the range is extended to ~150mm.

I. Signal distortions in the focuser's vicinities

To analyze the distortion of the magnetic field by the highly permeable cores of the focuser, several FEM simulations with the above setup were performed. The distortion was determined by evaluation of the magnetic field along 1D parameter curves, referred to as sensing lines, in presence and absence of the focuser. In the simulations, the magnet was centrally positioned in a distance of 50mm from the core's surface, while the 200mm long sensing lines were placed parallel to the cores in the x-y plane on both sides of the focuser, in distances of ±25mm and -50mm, as depicted in Fig. 16.

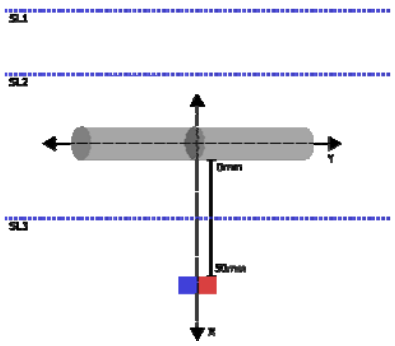

Figure 16. Sketch of the measurements for detecting the signal distortions in the focuser's vicinities

To get a feeling for the amplification effect of the above setup, the magnetic field was determined in the sensing area in presence and absence of the cores. In the first case the y-component of the field is ~2.14mT, while in the second case it drops to ~0.115mT with less than 1% simulation error, which corresponds to an increase of the signal by a factor of approximately 18.5 due to the presence of the focuser.

Fig. 17 to 19 (a) show the y-component of the magnetic field referred to as the signal in presence and absence of the field focuser along the three sensing lines, while in (b) the absolute differences between the two are shown.

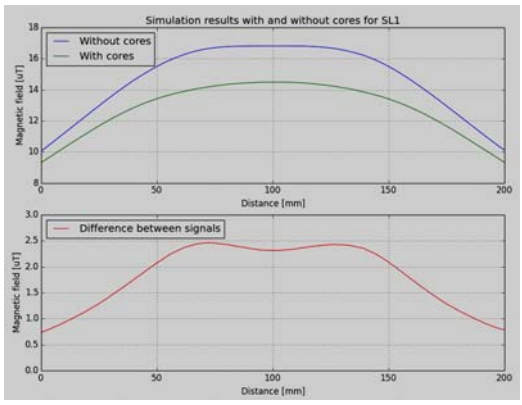

Figure 17. (a) Signal with and without focuser, (b) Difference between signals for the sensor line SL1

The concave behavior of the undistorted field (blue) along sensor line SL1, that is expected for the far field of any magnet with similar orientation, is clearly visible. The green trace shows, that the magnetic field is reduced by the core, which can be interpreted as a shielding effect that the permeable cores exhibit in the region opposite of the magnetic source. The difference signal in (b) shows a clear double peak, which is a result of the length of the focuser that functions as a long permanent magnet which mainly generates a field at its edges. Similar effects can also be observed along SL2, shown in Fig. 18.

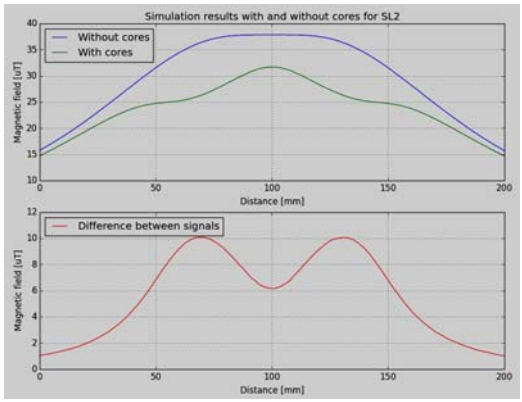

Figure 18. (a) Signal with and without focuser, (b) Difference between signals for the sensor line SL2

While the general behavior of the magnetic field along SL2 is reminiscent of the one along SL1, the distortion of the field is much more pronounced in shape and amplitude as SL2 lies much closer to the ferrite cores.

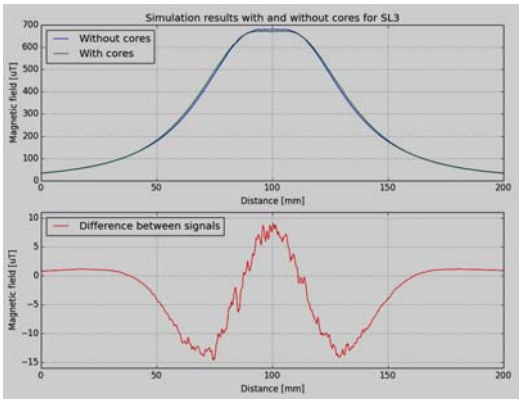

Figure 19. (a) Signal with and without focuser, (b) Difference between signals for the sensor line SL3

In contrast to SL1 and SL2, the sensor line SL3 lies on the opposite side of the ferrite cores, in-between the magnet and the focuser. The shielding effect is reversed on this side as the permeable cores attempt to draw more field into this region, initiating a magnetic circuit between themselves and the magnet.

Generally one can conclude from Fig. 17 to 19 that the focuser attempts to draw in the magnetic fields from its surroundings, enhances them in the core and focuses them in the gap where the sensor can be placed beneficially.

For improved understanding, Fig. 20 shows 3D plots of the y-component of the magnetic field along the sensing line SL2 in presence and absence of the focuser for airgap variations from X=10mm to X=190mm. While the above analysis holds, the airgap variation seems to be mainly responsible for a change in amplitude as well as the width of the peaks, an expected effect resulting from the distance from the source. The closer the magnet is to the focuser the stronger the shielding effect.

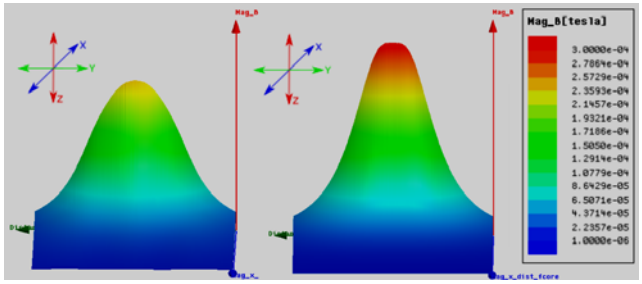

Figure 20. 3D plot of the y-component of the magnetic field (a) in absence and (b) presence of the focuser along the sensor line SL2 (Y) and airgap variations (X) from 10mm to 190mm.

In addition to the variation of the airgap, in Fig. 21 the y-component of the magnetic field along SL2 is depicted for a transversal movement of the magnet, i.e. for a constant airgap parallel to the sensing lines. The airgap is fixed to X=50mm while the magnet is moved within a range of Y=±100mm from the center.

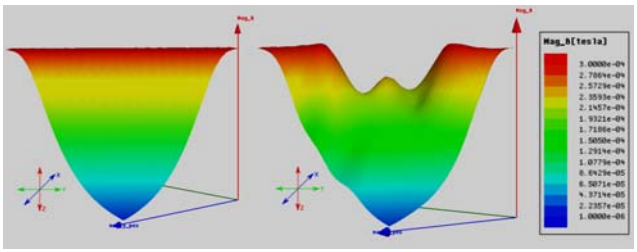

Figure 21. 3D plot of the y-component of the magnetic field (a) in absence and (b) presence of the focuser along the sensor line SL2 (X) and variation of the transversal position of the magnet (Y) from -100mm to 100mm.

In absence of the focuser, the decay of the field along the sensing line is clearly visible together with the shift of the peak with the transversal position of the magnet. The distortion behavior becomes quite complicated in presence of the focuser. It can be observed, that when the magnet is "outside" of the range of the focuser (±46,5mm), the field seems to be only slightly distorted as if there was no or only little shielding effect. Inside the critical range (within the focuser's boundaries) however, the distortion appears rapidly and is strong. It seems that the geometric range of the distortion of the focuser, which describes also the shielding effect, depends not only on the size and shape of the latter, but also on the position of the source of the magnetic field.

V. CONCLUSION

It was shown, that with the help of a field focuser the magnetic field can be enhanced by several orders of magnitude. In the context of magnetic position detection this is a useful and cost-effective solution to compensate the fast decay of the field of permanent magnets when combined with low sensitivity Hall sensor technology. In addition, the influence on the magnetic field in the surroundings of the focusing device was studied in detail.

The main advantage of the proposed system lies in bridging the gap to other more sensitive magnetic field detection technologies like GMR or TMR in a highly cost effective manner, providing all the advantages of modern Hall sensors that include wide measurement ranges, linearity and sophisticated on chip signal processing techniques for temperature and pressure compensation.

Future studies aim to shed light on the connection between specific movement types and geometric implementations of the focuser to understand the limits and to provide optimal solutions for position and orientation detection systems.

ACKNOWLEDGMENT

This project has been supported by the COMET K1 center ASSIC - Austrian Smart Systems Integration Research Center. The COMET - Competence Centers for Excellent Technologies Program is supported by BMVIT, BMWFW and the federal provinces of Carinthia and Styria.

REFERENCES

[1] M. Ribeiro, M. Ortner, and M. Seger, "Long range magnetic field measurement with magnetic sensors", in Proceedings of the International Conference on Industrial Automation, Information and

Communications Technology (IAICT 2014), A. H. Gunawan, Ed., Telkom Indonesia, pp. 97–103. DOI: 10.1109/IAICT.2014.6922090.

[2] M. Ribeiro, "Influence Analysis of a Magnetic Field Focusing Device for Long Range Position Detection Measurement", in Proceedings of the 18th International Conference on Modeling and Simulation (UKSIm-AMSS), IEEE Conference Publication Services, ISBN 978-1-5090-0887-2.

[3] E. Hall, "On a New Action of the Magnet on electric Currents", American Journal of Mathematics 2: 287-292, 1879.

[4] T. Bratland, M. J. Caruso, R. W. Schneider, "A New Perspective on Magnetic Field Sensing", Sensors, 1998.

[5] D. Niarchos, "Magnetic MEMS: key issues and some applications", Sensors and Actuators A: Physical 106, 1-3: 255-262, 2003.

[6] A. Fert, "The origin, development and future of spintronics", Soviet Physics Uspekhi 178, 12: 1336-1348, 2008.

[7] J. Lenz and A.S. Edelstein, "Magnetic Sensors and their Applications", IEEE Sens. J. 6: 631-649, 2006.

[8] M. Diaz-Michelena, "Small Magnetic Sensors for Space Applications", Sensors 9: 2271-2288, 2009.

[9] Melexis, "Magnets for MLX90333 linear position sensor", Appl. Note 90333-LP-AP-041007, 2007

[10] D. J. Griffiths, "Introduction to Electrodynamics", 1999, Prentice-Hall, Inc. Upper Saddle River, New Jersey 07458.

[11] A. R. Hambley, "Electrical Engineering: Principles and Applications", 4th ed., Pearson Education, Inc., 2008.

[12] R. Popovics and C. Schott, "Magnetic field sensor and method for operating the magnetic field sensor", US 7259556 B2, 2007

[13] H. Blanchard et al. "Highly sensitive Hall sensor in CMOS technology." Sensors and Actuators A: Physical 82.1 (2000): 144-148.

[14] ANSYS Maxwell, User's Guide - Maxwell 2D, ANSYS Inc., Canonsburg, PA, March 2011.

[15] Poole, G., Liu, Y. C., & Mandel, J. (2003). Advancing analysis capabilities in ANSYS through solver technology. *Electronic Transactions on Numerical Analysis*, *15*, 106-121.

[16] M. Ribeiro, M. Ortner, and M. Seger, "Long range magnetic field measurement with magnetic sensors", in Proceedings of the International Conference on Industrial Automation, Information and Communications Technology (IAICT 2014), A. H. Gunawan, Ed., Telkom Indonesia, pp. 97–103. DOI: 10.1109/IAICT.2014.6922090.

[17] Melexis, "Precision Programmable Linear Hall Effect Sensor", MLX90215 datasheet, Sep. 2003.

[18] Wuntronic GmbH, "Tesla Meter / Gauss Meter with USB Interface and Analog Output", Koshava 5 datasheet, 2011.